Science Journal of Circuits, Systems and Signal Processing
2025, Vol. 12, No. 2, pp. 16–29
https://doi.org/10.11648/j.cssp.20251202.11

Research Article

Image Reconstruction in Compressive Sensing Using Biorthogonal 5.5 (bior5.5) and Lifting Wavelet Transforms with SP, CoSaMP, and ALISTA Algorithms

Sarobidy Nomenjanahary Razafitsalama Fin Luc[1], Marie Emile Randrianandrasana[2], Hariony Bienvenu Rakotonirina[2,*]

[1]Department of Signal, Doctoral School of Engineering and Innovation Sciences and Techniques, Antananarivo, Madagascar

[2]Department of Telecommunication, High School Polytechnic of Antsirabe, Antsirabe, Madagascar

Abstract

This paper proposes an efficient image reconstruction for compressive sensing (CS) that combines the Lifting Wavelet Transform (LWT) using Biorthogonal 5.5 (bior5.5) wavelets with three reconstruction algorithms: Subspace Pursuit (SP), Compressive Sampling Matching Pursuit (CoSaMP), and the Analytic Learned Iterative Shrinkage Thresholding Algorithm (ALISTA). Unlike the conventional Discrete Wavelet Transform (DWT) which relies on computationally intensive convolution operations the LWT provides a faster sparse representation while preserving the sparsity crucial for CS. The proposed approach leverages a key insight: among the four subbands produced by the LWT namely the approximation (CA) and the detail coefficients (LH, HL, HH) only the latter three are inherently sparse. Therefore, compressive sensing is applied exclusively to these detail subbands, while the CA subband is left uncompressed to retain essential low-frequency information. Experiments were conducted on both a natural test image (Lena) and a medical MRI scan, across image resolutions ranging from 200×200 to 512×512 pixels and sampling rates from 10% to 80%. Performance was assessed using the Structural Similarity Index (SSIM) and reconstruction time. Results consistently demonstrate that ALISTA significantly outperforms SP and CoSaMP in both reconstruction fidelity and computational efficiency. At an 80% sampling rate, ALISTA achieves SSIM values of 0.99409 for Lena and 0.9775 for the MRI image, compared to approximately 0.96 and 0.95644, respectively, for the other two methods. Furthermore, ALISTA maintains remarkably low reconstruction times under 4 seconds even for 512×512-pixel images. These findings confirm that the ALISTA + LWT/bior5.5 combination offers the best trade-off between image quality and speed, exhibiting robustness across different image types and scales.

Keywords

Compressive Sensing, Biorthogonal, Subspace Pursuit, Wavelet Transform

*Corresponding author: dao.rakotonirina@gmail.com (Hariony Bienvenu Rakotonirina)

Received: 20 October 2025; **Accepted:** 3 November 2025; **Published:** 19 December 2025

1. Introduction

Image reconstruction from a limited number of measurements remains a significant challenge in critical domains such as data compression, medical imaging, remote sensing, and embedded vision systems applications where real-time processing and stringent hardware resource constraints pose particularly demanding requirements. Compressive Sensing (CS) offers a powerful theoretical framework to tackle this problem by leveraging the inherent sparsity of signals in appropriate transform domains, especially wavelet bases [1]. Traditionally, the Discrete Wavelet Transform (DWT) has been employed to obtain such sparse representations; however, its standard implementation using convolutional filter banks entails high computational complexity and latency, substantially limiting its suitability for applications requiring rapid reconstruction. To address these drawbacks, this work adopts the Lifting Wavelet Transform (LWT) a reformulation of the DWT that enables a faster implementation while retaining the sparsity properties crucial for CS. We propose an image reconstruction method based on a level-1 LWT using Biorthogonal 5.5 (bior5.5) wavelets, integrated with three iterative reconstruction algorithms: Subspace Pursuit (SP), Compressive Sampling Matched Pursuit (CoSaMP), and the Analytic Learned Iterative Shrinkage Thresholding Algorithm (ALISTA). Our goal is to evaluate and compare their performance in terms of reconstruction quality measured by the Structural Similarity Index (SSIM) and computational efficiency across sampling rates ranging from 10% to 80%. Using both the standard Lena test image and a Magnetic Resonance Imaging (MRI) scan under consistent experimental conditions, this study seeks to identify the most effective algorithmic combination for practical compressive sensing applications, where both reconstruction speed and fidelity are simultaneously critical [2].

2. Principle of Compressive Sensing Applied to an Image

2.1. Lifting Wavelet Transform Phase

The Lifting Wavelet Transform (LWT) is an efficient reformulation of the Discrete Wavelet Transform (DWT), designed to reduce computational complexity while preserving the sparsity properties essential for sparse signal representation.

The Lifting Wavelet Transform (LWT) is based on a three-step decomposition process:

1) *Split:* The input signal is divided into two subsequences typically even and odd indexed samples.
2) *Predict*: Odd samples are predicted from the even ones using a prediction operator, the difference between the prediction and the actual odd samples yields the detail coefficients (high-frequency components).
3) *Update*: The even samples are updated using the detail coefficients to produce the approximation coefficients (low-frequency components), while preserving certain global properties of the original signal (such as its average).

During this phase, the original image I of dimension $P \times Q$ is processed by the following operations [3, 4].

1) Initialization

$M \leftarrow number\ of\ rows\ of\ I$

$N \leftarrow number\ of\ columns\ of\ I$

$p \leftarrow [4.9933, 4.9933, 5.5858, 5.5858, 0.2901]$

$u \leftarrow [-0.1834, -0.0044, -3.0949, 0.1732, -3.4472]$

2) Horizontal decomposition (row by row)

For each row $i = 0$ to $M-1$:

Splitting

$$s[k] \leftarrow I[i, 2k]\ \forall\ k = 0, \dots, K_s - 1$$

where $K_s \leftarrow \lceil N/2 \rceil$

$$d[k] \leftarrow I[i, 2k+1]\ \forall\ k = 0, \dots, K_d - 1$$

where $K_d \leftarrow \lfloor N/2 \rfloor$

Symmetric padding of s

$$\tilde{s} \leftarrow sym\_pad(s, left = 4, right = 4)$$

Predict step

$$pred[k] \leftarrow \sum_{m=0}^{4} p[m].\tilde{s}[k+m-3]\ \forall\ k = 0, \dots, K_d - 1$$

$$d[k] \leftarrow d[k] - pred[k]$$

Symmetric padding of d

$$\tilde{d} \leftarrow sym\_pad(d, left = 4, right = 4)$$

Update step

$$updt[k] \leftarrow \sum_{m=0}^{4} u[m].\tilde{d}[k+m-3]\ \forall\ k = 0, \dots, K_d - 1$$

$$s[k] \leftarrow s[k] + updt[k]$$

Horizontal recombination

$$H[i, 0{:}K_s - 1] \leftarrow s$$

$$H[i, K_s{:}K_s + K_d - 1] \leftarrow d$$

3) Vertical decomposition (column by column of H)

Temporarily transpose: H^T

For each column $j = 0$ to $(K_s + K_d) - 1$:

Splitting

$$s[k] \leftarrow H^T[2k, j]\ \forall\ k = 0, \ldots, L_s - 1$$

where $L_s \leftarrow \lceil M/2 \rceil$

$$d[k] \leftarrow H^T[2k+1, j]\ \forall\ k = 0, \ldots, L_d - 1$$

where $L_d \leftarrow \lfloor M/2 \rfloor$

Symmetric padding of $s \rightarrow \tilde{s}$

Predict

$$pred[k] \leftarrow (p * \tilde{s})[k+3]$$

$$d[k] \leftarrow d[k] - pred[k]$$

Symmetric padding of $d \rightarrow \tilde{d}$

Update

$$updt[k] \leftarrow (u * \tilde{d})[k+3]$$

$$s[k] \leftarrow s[k] + updt[k]$$

Vertical recombination

$$V^T[0{:}\,L_s - 1, j] \leftarrow s$$

$$V^T[L_s{:}\,L_s + L_d - 1, j] \leftarrow d$$

Re-transpose: $T \leftarrow V$

Subband extraction

$$cA \leftarrow T[0{:}\,L_s - 1, 0{:}\,K_s - 1]$$

$$lh \leftarrow T[0{:}\,L_s - 1, K_s{:}\,K_s + K_d - 1]$$

$$hl \leftarrow T[L_s{:}\,L_s + L_d - 1, 0{:}\,K_s - 1]$$

$$hh \leftarrow T[L_s{:}\,L_s + L_s - 1, K_s{:}\,K_s + K_s - 1]$$

2.2. Acquisition or Measurement Phase

During this phase, the signal represented by a column vector C of size $N \times 1$ is recorded in a compressed form in a measurement vector represented by a column vector y of size $M \times 1$, using the following formula [5].

$$y = AC \tag{1}$$

Where:

A is a rectangular matrix of size $M \times N$, known as the measurement matrix $(M < N)$

$C = lh, hl, hh$

2.3. Reconstruction Phase

During this phase, the goal is to find the vector C that satisfies Equation (1). Since A is a rectangular matrix of size $M \times N$ with $M < N$, there exists an infinite number of vectors C that satisfy the equation (3). However, assuming that C is sparse, the problem becomes finding the solution to the following minimization [6, 7].

$$\hat{C} = arg\ min\|C\|_0 \text{ subject to } y = AC \tag{2}$$

2.4. Inverse Lifting Wavelet Transform Phase

The principle of the inverse Lifting Wavelet Transform (inverse LWT) is to reconstruct the original signal from the approximation and detail coefficients by applying the LWT steps in reverse order and with inverse operations:

1) *Undo Update*: The approximation coefficients are used to recover the original even-indexed samples by reversing the update operation.
2) *Undo Predict*: The detail coefficients are added back to the reconstructed even samples to retrieve the original odd-indexed samples, thereby inverting the predict operation.
3) *Merge:* The even and odd samples are interleaved to fully reconstruct the original signal.

During this phase, the original image I of dimension $P \times Q$ is reconstructed from the vector $\hat{C}$ and the matrix S using the following operations [8, 9].

1) Initialization

$$L_s \leftarrow number\ of\ rows\ of\ cA$$

$$K_s \leftarrow number\ of\ columns\ of\ cA$$

$$L_d \leftarrow number\ of\ rows\ of\ hl$$

$$K_d \leftarrow number\ of\ columns\ of\ lh$$

$$T \leftarrow \begin{bmatrix} cA & lh \\ hl & hh \end{bmatrix}$$

$$p \leftarrow [4.9933, 4.9933, 5.5858, 5.5858, 0.2901]$$

$$u \leftarrow [-0.1834, -0.0044, -3.0949, 0.1732, -3.4472]$$

2) Vertical reconstruction (column by column of T)

Temporarily transpose: T^T

For each column $j = 0$ to $(K_s + K_d) - 1$:

Split subbands

$$s[k] \leftarrow T^T[k, j]\ \forall\ k = 0, \ldots, L_s - 1$$

$$d[k] \leftarrow T^T[L_s + k, j]\ \forall\ k = 0, \ldots, L_d - 1$$

Symmetric padding of d

$$\tilde{d} \leftarrow sym\_pad(d, left = 4, right = 4)$$

Undo Update step

$$updt[k] \leftarrow \sum_{m=0}^{4} u[m].\tilde{d}[k+m-3] \ \forall\, k = 0, \ldots, L_s - 1$$

$$s[k] \leftarrow s[k] - updt[k]$$

Symmetric padding of s

$$\tilde{s} \leftarrow sym\_pad(s, left = 4, right = 4)$$

Undo Predict step

$$pred[k] \leftarrow \sum_{m=0}^{4} p[m].\tilde{s}[k+m-3] \ \forall\, k = 0, \ldots, L_d - 1$$

$$d[k] \leftarrow d[k] + pred[k]$$

Merge (interleave) to reconstruct column
Initialize $col\_rec \in \mathbb{R}^{L_s+L_d}$

$$col\_rec[2k] \leftarrow s[k] \ \forall\, k = 0, \ldots, L_s - 1$$

$$col\_rec[2k+1] \leftarrow d[k] \ \forall\, k = 0, \ldots, L_d - 1$$

$$V^T[0{:}\, L_s + L_d - 1, j] \leftarrow col\_rec$$

Re-transpose: $H_{rec} \leftarrow V$
3) Horizontal reconstruction (row by row of H_{rec})
For each row $i = 0$ to $(L_s + L_d) - 1$:
Split subbands

$$s[k] \leftarrow H_{rec}[i, k] \ \forall\, k = 0, \ldots, K_s - 1$$

$$d[k] \leftarrow H_{rec}[i, K_s + k] \ \forall\, k = 0, \ldots, K_d - 1$$

Symmetric padding of d

$$\tilde{d} \leftarrow sym\_pad(s, left = 4, right = 4)$$

Undo Update step

$$updt[k] \leftarrow \sum_{m=0}^{4} u[m].\tilde{d}[k+m-3] \ \forall\, k = 0, \ldots, K_s - 1$$

$$s[k] \leftarrow s[k] - updt[k]$$

Symmetric padding of s

$$\tilde{s} \leftarrow sym\_pad(s, left = 4, right = 4)$$

Undo Predict step

$$pred[k] \leftarrow \sum_{m=0}^{4} p[m].\tilde{s}[k+m-3] \ \forall\, k = 0, \ldots, K_d - 1$$

$$d[k] \leftarrow d[k] + pred[k]$$

Merge (interleave) to reconstruct row
Initialize $row\_rec \in \mathbb{R}^{K_s+K_d}$

$$row\_rec[2k] \leftarrow s[k] \ \forall\, k = 0, \ldots, K_s - 1$$

$$row\_rec[2k+1] \leftarrow d[k] \ \forall\, k = 0, \ldots, K_d - 1$$

$$\hat{I}[0{:}\, L_s + L_d - 1, j] \leftarrow row\_rec$$

3. Metric for Evaluating Reconstruction Quality

3.1. Mean Squared Error (MSE)

The following provides its definition [10, 11].

$$MSE = \frac{1}{P \times Q} \sum_{i=0}^{P-1} \sum_{j=0}^{Q-1} \left(I_{ij} - \hat{I}_{ij}\right)^2 \tag{3}$$

Where:
MSE denotes the Mean Squared Error
P denotes the number of rows of the image
Q denotes the number of colomuns of the image
I_{ij} denotes the pixel value at position (i, j) in the original image
$\hat{I}_{ij}$ denotes the pixel value at position (i, j) in the reconstructed image

3.2. Peak Signal-to-noise Ratio (PSNR)

The following provides its definition [12, 13].

$$PSNR = 10\, log_{10}\left(\frac{65025}{MSE}\right) \tag{4}$$

Where:
$PSNR$ denotes the Peak Signal-to-Noise Ratio
MSE denotes the Mean Squared Error

3.3. Structural Similarity Index (SSIM)

The following provides its definition [14, 15].

$$SSIM(x, y) = \frac{(2\mu_x\mu_y + C_1)(2\sigma_{xy} + C_2)}{({\mu_x}^2 + {\mu_y}^2 + C_1)({\sigma_x}^2 + {\sigma_y}^2 + C_2)} \tag{5}$$

Where:
$SSIM$ denotes the Structural Similarity Index
μ_x denotes the mean intensity value of image x
μ_y denotes the mean intensity value of image y
σ_x denotes the variance of image x
σ_y denotes the variance of image y
σ_{xy} denotes the covariance between x and y

$$C_1 = (K_1 L)^2$$

$$C_2 = (K_2 L)^2$$

L denotes the dynamic range of pixel values

$$K_1 = 0.01$$

$$K_2 = 0.03$$

4. Comparison of the Original and Reconstructed Images

In this section, the following points are specified:

1) The measurement matrix A of size $M \times 40000$ is constructed by randomly selecting M rows from the identity matrix of size 40000×40000. It is a Gaussian measurement matrix. We selected it for its excellent statistical properties (RIP ou Restricted Isometry Property, incoherence), which are essential in compressive sensing.
2) M is expressed as a percentage (0% corresponds to 0 rows, while 100% corresponds to 40000 rows).
3) The resolution of Equation (2) is carried out using the Subspace Pursuit (SP) algorithm
4) The Mean Squared Error (MSE) is computed using Equation (3)
5) The Peak Signal-to-Noise Ratio (PSNR) is computed using Equation (4)
6) The Structural Similarity Index (SSIM) is computed using Equation (5)
7) Processed image:

Lena excerpted from the original publication: A. K. Jain, Fundamentals of Digital Image Processing, Prentice-Hall, 1989, p. 400. Original source: photograph from Playboy magazine, November 1972. Used here for non-commercial educational and research purposes.

Figure 1. *Processed image (Lena).*

We also processed a free medical MRI image available on iStockphoto.com, which offers royalty-free visual content. This image is available at this link:

https://www.istockphoto.com/fr/photo/cerveau-gm182682597-12321941?searchscope=image%2Cfilm

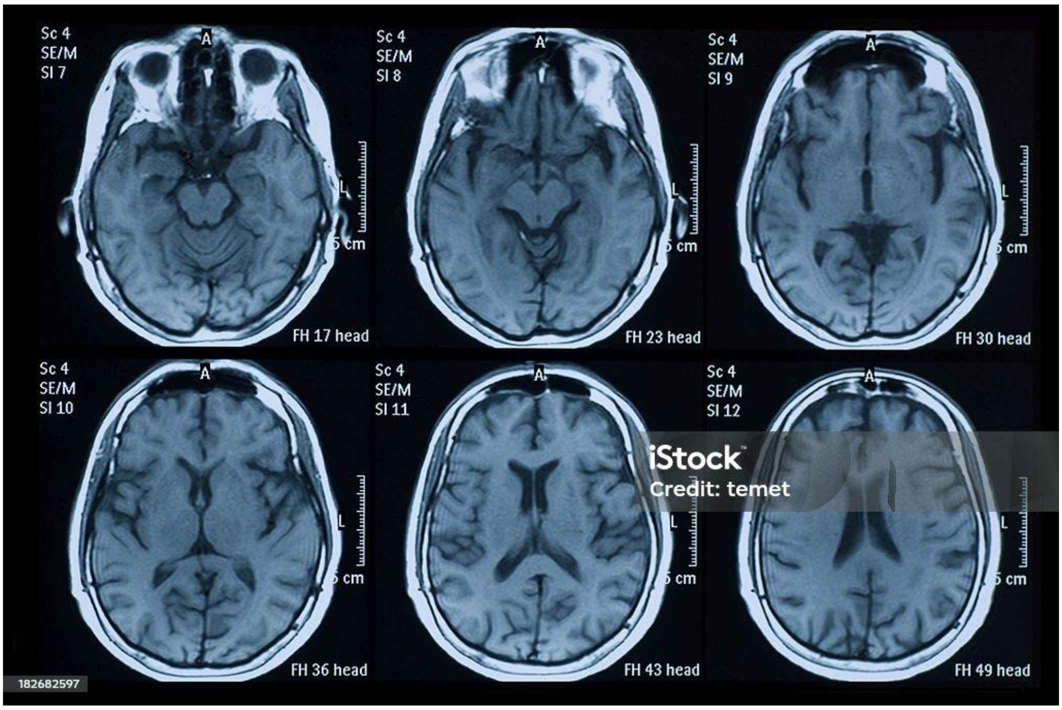

Figure 2. *Processed image (MRI).*

1) Image size: 200×200 pixels, 256×256 pixels, 300×300 pixels, 400×400 pixels and 512×512 pixels
2) Programming environment: MATLAB 2023
3) Hardware specifications: CPU: Intel(R) Core i7-9750H, GPU: NVIDIA GetForce RTX 2060, RAM: 16Go

There are two experimental scenarios:

1) Scenario 1: Performance evaluation of the proposed algorithms across different sampling rates and on two distinct images. The performance metrics are the Structural Similarity Index (SSIM) and image reconstruction time. Note that the image size was fixed at 200 × 200 pixels.
2) Scenario 2: Performance evaluation of the proposed algorithms on images of varying sizes (256 × 256, 300 × 300, 400 × 400, and 512 × 512 pixels), with the sampling rate fixed at 30%. This value was chosen to assess whether our algorithms can still successfully reconstruct the image even from a relatively small number of measurements. The experiment is again conducted on two different images, using SSIM and reconstruction time as performance criteria.

Table 1 presents the images reconstructed by the CoSaMP, SP, and ALISTA algorithms for sampling rates ranging from 10% to 80%.

Table 1. *Images reconstructed for Lena image (scenario 1).*

M (%)	CoSaMP	SP	ALISTA
10	 SSIM=0.94281 Time(minute)=0.022691	 SSIM=0.94281 Time(minute)=0.01611	 SSIM=0.94281 Time(minute)=0.011124
20	 SSIM=0.94733 Time(minute)=0.032437	 SSIM=0.94733 Time(minute)=0.053624	 SSIM=0.94764 Time(minute)=0.017857
30	 SSIM=0.95854 Time(minute)=0.10569	 SSIM=0.95854 Time(minute)=0.092759	 SSIM=0.96022 Time(minute)=0.02277
40	 SSIM=0.96653 Time(minute)=0.34529	 SSIM=0.96653 Time(minute)=0.14001	 SSIM=0.97153 Time(minute)=0.031965

M (%)	CoSaMP	SP	ALISTA
50	 SSIM=0.97013 Time(minute)=0.33287	 SSIM=0.97013 Time(minute)=0.06803	 SSIM=0.97875 Time(minute)=0.041312
60	 SSIM=0.97212 Time(minute)=0.12799	 SSIM=0.97212 Time(minute)=0.077623	 SSIM=0.98353 Time(minute)=0.054415
70	 SSIM=0.97358 Time(minute)=0.14835	 SSIM=0.97358 Time(minute)=0.090664	 SSIM=0.98735 Time(minute)=0.047454
80	 SSIM=0.97662 Time(minute)=0.16927	 SSIM=0.97662 Time(minute)=0.10228	 SSIM=0.99409 Time(minute)=0.06381

The results obtained are summarized in Table 2.

Table 2. *Summary of the results for Lena image (scenario 1).*

M(%)	SSIM			Reconstruction Time (minute)		
	CoSaMP	**SP**	**ALISTA**	**CoSaMP**	**SP**	**ALISTA**
10%	0.94281	0.94281	0.94281	0.022691	0.01611	0.011124
20%	0.94733	0.94733	0.94764	0.032437	0.053624	0.017857
30%	0.95854	0.95854	0.96022	0.10569	0.092759	0.02277
40%	0.96653	0.96653	0.97153	0.34529	0.14001	0.031965
50%	0.97013	0.97013	0.97875	0.33287	0.06803	0.041312

M (%)	**SSIM**			**Reconstruction Time (minute)**		
	CoSaMP	**SP**	**ALISTA**	**CoSaMP**	**SP**	**ALISTA**
60%	0.97212	0.97212	0.98353	0.12799	0.077623	0.054415
70%	0.97358	0.97358	0.98735	0.14835	0.090664	0.047454
80%	0.97662	0.97662	0.99409	0.16927	0.10228	0.06381

Table 3 presents the images reconstructed by the CoSaMP, SP, and ALISTA algorithms for sampling rates ranging from 10% to 80% for MRI image.

Table 3. *Images reconstructed for MRI Image (scenario 1).*

M (%)	**CoSaMP**	**SP**	**ALISTA**
10	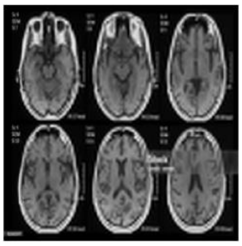 SSIM=0.89175 Time(minute)=0.011285	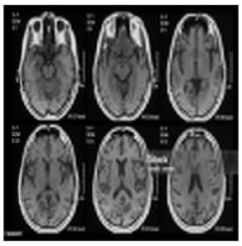 SSIM=0.89175 Time(minute)=0.011991	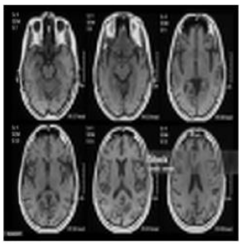 SSIM=0.89175 Time(minute)=0.0034434
20	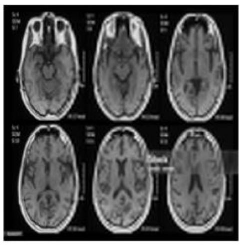 SSIM=0.90249 Time(minute)=0.014772	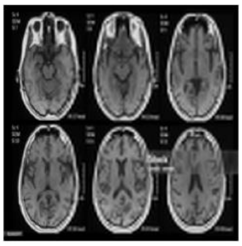 SSIM=0.90249 Time(minute)=0.013637	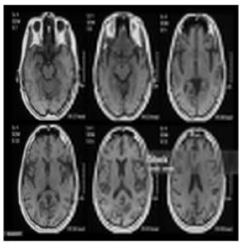 SSIM=0.90291 Time(minute)=0.0034373
30	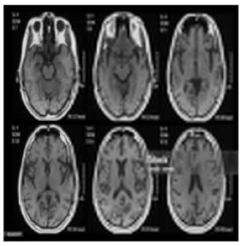 SSIM=0.91075 Time(minute)=0.016735	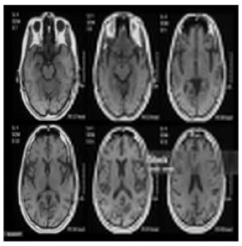 SSIM=0.91075 Time(minute)=0.014157	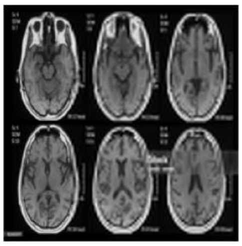 SSIM=0.91379 Time(minute)=0.0033874
40	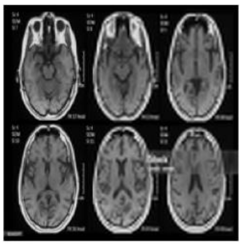 SSIM=0.91851 Time(minute)=0.017691	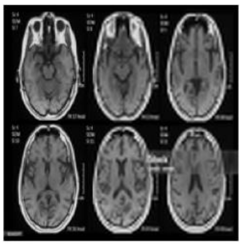 SSIM=0.91851 Time(minute)=0.016461	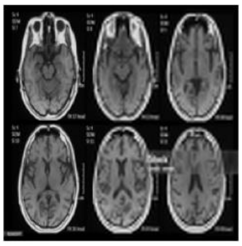 SSIM=0.92567 Time(minute)=0.0034083

M (%)	CoSaMP	SP	ALISTA
50	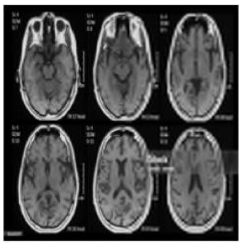 SSIM=0.92705 Time(minute)=0.019187	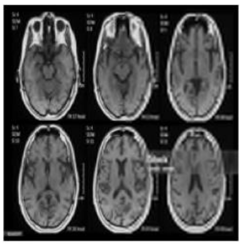 SSIM=0.92705 Time(minute)=0.018123	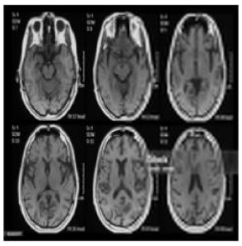 SSIM=0.94022 Time(minute)=0.0034876
60	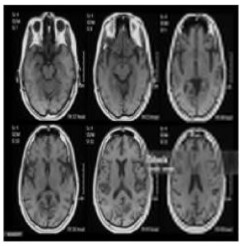 SSIM=0.93008 Time(minute)=0.020836	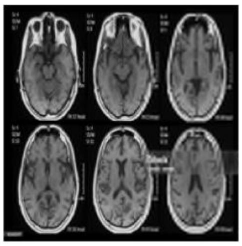 SSIM=0.93008 Time(minute)=0.019408	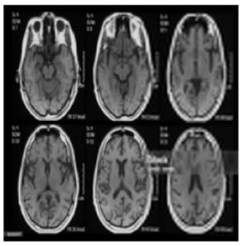 SSIM=0.95084 Time(minute)=0.0035112
70	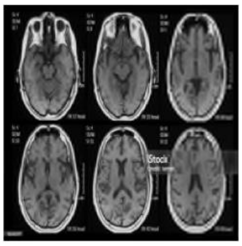 SSIM=0.93636 Time(minute)=0.022816	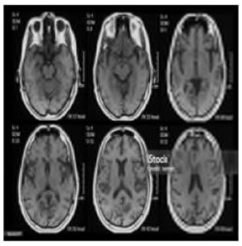 SSIM=0.93636 Time(minute)=0.022256	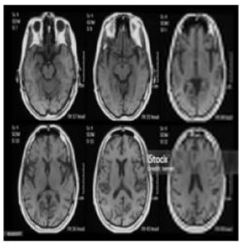 SSIM=0.96478 Time(minute)=0.0035289
80	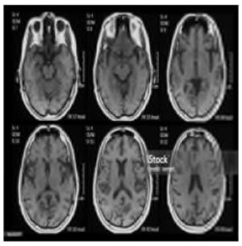 SSIM=0.94089 Time(minute)=0.024535	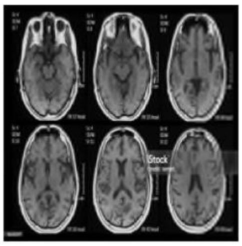 SSIM=0.94089 Time(minute)=0.023184	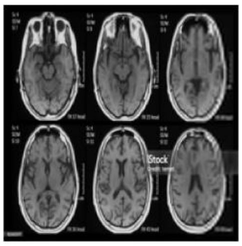 SSIM=0.9775 Time(minute)=0.0034404

The results obtained are summarized in Table 4.

Table 4. *Summary of the results for MRI Image (scenario 1).*

M(%)	SSIM			Reconstruction Time (minute)		
	CoSaMP	SP	ALISTA	CoSaMP	SP	ALISTA
10%	0.89175	0.89175	0.89175	0.011285	0.011991	0.0034434
20%	0.90249	0.90249	0.90291	0.014772	0.013637	0.0034373
30%	0.91075	0.91075	0.91379	0.016735	0.014157	0.0033874
40%	0.91851	0.91851	0.92567	0.017691	0.016461	0.0034083

M(%)	SSIM			Reconstruction Time (minute)		
	CoSaMP	SP	ALISTA	CoSaMP	SP	ALISTA
50%	0.92705	0.92705	0.94022	0.019187	0.018123	0.0034876
60%	0.93008	0.93008	0.95084	0.020836	0.019408	0.0035112
70%	0.93636	0.93636	0.96478	0.022816	0.022256	0.0035289
80%	0.94089	0.94089	0.9775	0.024535	0.023184	0.0034404

In order to interpret the results, we decided to present these values in the form of curves (Figures 3 and 4).

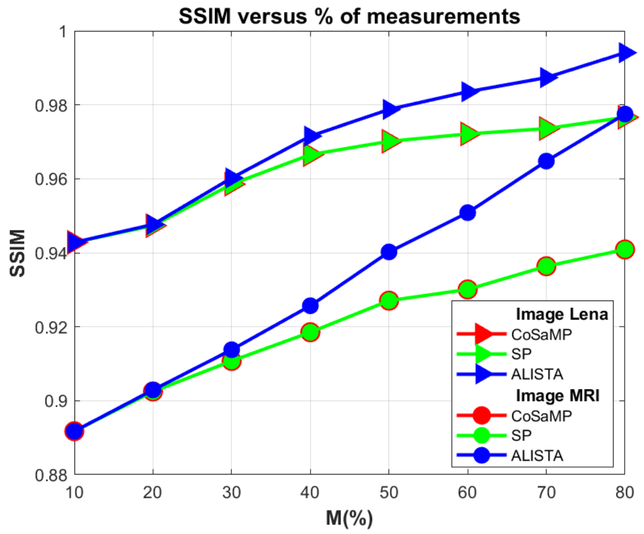

Figure 3. *SSIM vs% of measurements.*

Figure 3 compares the performance of three image reconstruction algorithms in terms of image quality, as quantified by the Structural Similarity Index (SSIM). The results are shown for two distinct image types: the standard Lena test image and an MRI scan. As expected, for all algorithms and both images, SSIM improves with an increasing percentage of measurements reflecting the intuitive principle that more acquired data leads to higher quality reconstructions. Notably, ALISTA consistently outperforms the other methods across both image types, achieving SSIM values of 0.9775 for the MRI image and 0.99409 for Lena. This superior performance can be attributed to ALISTA's learning-based nature. Unlike the greedy algorithms CoSaMP and SP, ALISTA learns optimal parameters from training data, allowing it to adapt effectively to the specific structural characteristics of the images.

Figure 4 displays the reconstruction time (in minutes) as a function of the percentage of measurements for the three algorithms CoSaMP, SP, and ALISTA applied to two image types: Lena (a natural image) and an MRI scan (a medical image). It is evident that ALISTA achieves an extremely low reconstruction time under 0.07 minutes (i.e., 4 seconds) regardless of the measurement rate or image type, establishing it as the most computationally efficient algorithm in terms of speed. In contrast, both CoSaMP and SP exhibit substantially longer reconstruction times that increase significantly with the number of measurements. This difference stems from the fundamentally distinct nature of these algorithms: ALISTA is based on a learning-based approach, whereas CoSaMP and SP are iterative greedy algorithms that require iterative selection and update steps whose convergence may vary depending on measurement density and image structure. Thus, ALISTA offers a dual advantage: high reconstruction quality (as previously demonstrated) and minimal computational cost, making it particularly well-suited for real-time or embedded applications where speed is critical.

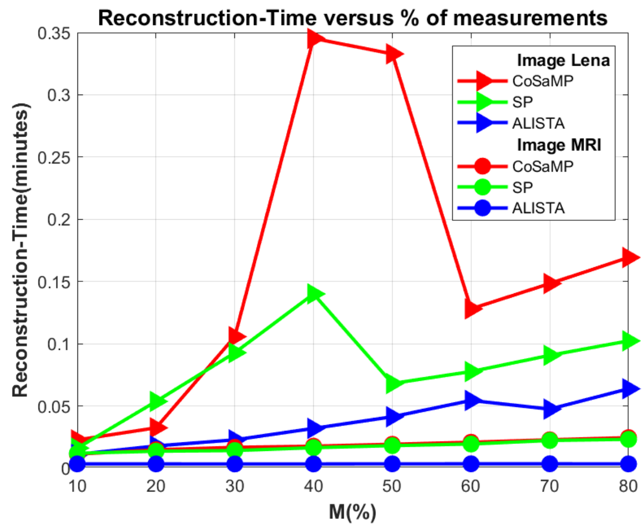

Figure 4. *Reconstruction time vs% of measurements.*

For the second scenario, Tables 5 and 6 show the evaluation of the algorithms across different image sizes.

***Table 5**. Summary of the results for Lena Image (scenario 2).*

Image size	SSIM			Reconstruction Time (minute)		
	CoSaMP	SP	ALISTA	CoSaMP	SP	ALISTA
256×256px	0.95804	0.95804	0.96179	0.028591	0.028783	0.006652
300×300px	0.95725	0.95725	0.96275	0.045994	0.042773	0.010911
400×400px	0.9586	0.9586	0.96691	0.10586	0.10283	0.027312
512×512px	0.96	0.96	0.97	0.22625	0.23957	0.067639

***Table 6**. Summary of the results for Lena Image (scenario 2).*

Image size	SSIM			Reconstruction Time (minute)		
	CoSaMP	SP	ALISTA	CoSaMP	SP	ALISTA
256×256px	0.92267	0.92267	0.92827	0.027767	0.027438	0.007279
300×300px	0.935	0.935	0.94133	0.046281	0.043884	0.010064
400×400px	0.94539	0.94539	0.95276	0.10503	0.10469	0.027045
512×512px	0.95644	0.95644	0.96327	0.22751	0.2349	0.066278

In order to interpret the results, we decided to present these values in the form of curves (Figures 5 and 6).

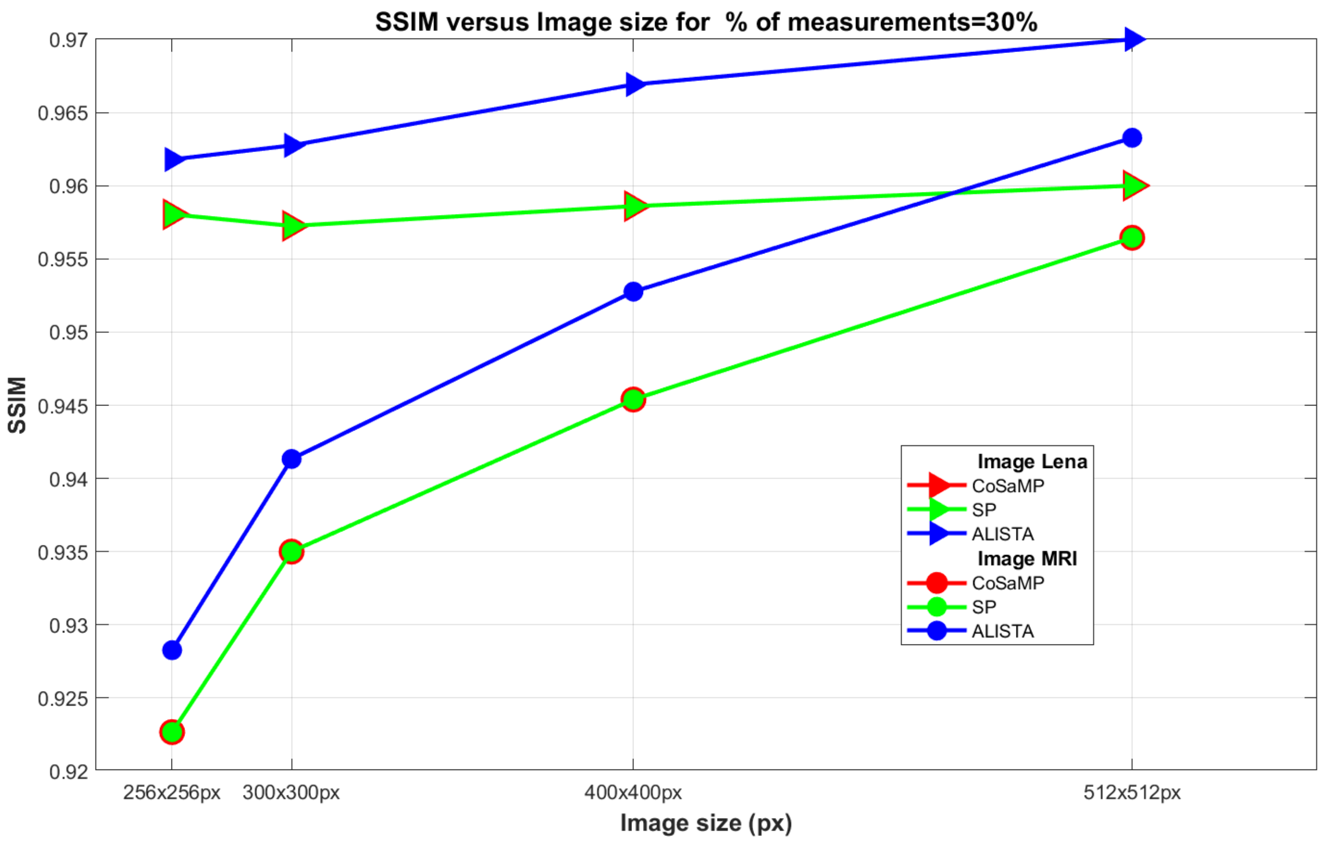

***Figure 5**. SSIM vs Image size for% of measurements=30%.*

Figure 5 shows the reconstruction quality, measured by SSIM, as a function of image size (in pixels) at a fixed measurement rate of 30%. For all algorithms and both image types, SSIM improves as image size increases a trend attributable to the richer structural detail and higher resolution available in larger images, which the algorithms can leverage more effectively. ALISTA consistently surpasses CoSaMP and SP across all tested resolutions and image types, achieving SSIM values above 0.97 for the Lena image and above 0.96 for the MRI scan at a resolution of 512×512 pixels. In comparison, CoSaMP and SP demonstrate lower reconstruction quality and greater sensitivity to variations in image content. Unlike classical greedy algorithms such as CoSaMP and SP, which rely heavily on iterative optimization, ALISTA uses predefined parameters (weight matrices and thresholds) learned from diverse image datasets, enabling robust reconstruction even on large-scale images.

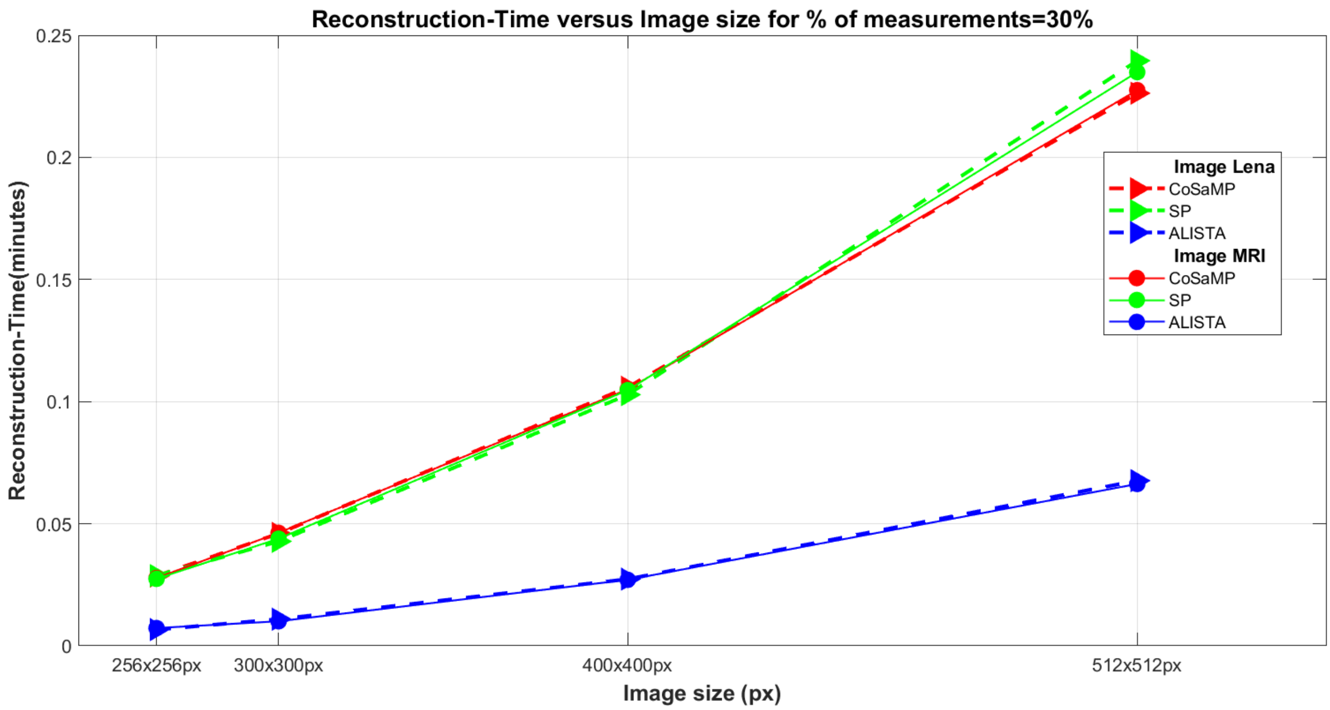

Figure 6. Reconstruction-Time vs Image size for % of measurements=30%.

Figure 6 presents the reconstruction time (in minutes) as a function of image size (in pixels) at a fixed measurement rate of 30%. ALISTA demonstrates an exceptionally low reconstruction time, staying under 0.07 minute (4 seconds) even for a 512×512-pixel image, which underscores its outstanding computational efficiency. In contrast, CoSaMP and SP exhibit substantially longer reconstruction times that rise sharply with increasing resolution, reaching nearly 0.23 minute (13 seconds). ALISTA is faster than CoSaMP and SP primarily because it relies on a deterministic and non-iterative architecture. Unlike CoSaMP and SP which are iterative greedy algorithms requiring, at each iteration, costly operations such as selecting the most correlated atoms, solving a least-squares problem over the estimated support, and updating the solution, ALISTA executes a fixed and predefined number of steps, where the weight matrices and thresholds are learned once and for all on a training dataset. Moreover, the reconstruction time for both Lena and MRI images is nearly identical for ALISTA, indicating that this algorithm is insensitive to image type and size.

5. Originality and Our Contribution to the Research

In compressive sensing, when processing images, the conventional Discrete Wavelet Transform (DWT) is typically used to obtain a sparse representation. However, this transform is computationally slow due to its convolution operations. In this paper, we propose a novel approach based on the Lifting Wavelet Transform (LWT) to address this limitation. Moreover, the originality and our key contribution lie in the methodology adopted for compressive sensing. Specifically, the LWT of an image yields four components:

1) CA: A reduced and blurred version of the original image
2) LH: Vertical details
3) HL: Horizontal details

4) HH: Diagonal details

According to our studies, the LH, HL, and HH components are inherently sparse matrices, unlike the CA component. This observation led us to apply compressive sensing only to these three detail components while leaving the CA component untouched. We therefore evaluated the performance of this proposed approach using various reconstruction algorithms. In this article, we use the Lifting Wavelet Transform (LWT) with the Biorthogonal 5.5 (bior5.5) wavelet.

6. Conclusion

In this paper, we propose an innovative image reconstruction method for Compressive Sensing (CS), combining the Lifting Wavelet Transform (LWT) using the biorthogonal bior5.5 wavelet basis with three iterative reconstruction algorithms: Subspace Pursuit (SP), Compressive Sampling Matched Pursuit (CoSaMP), and the Analytic Learned Iterative Shrinkage Thresholding Algorithm (ALISTA). Unlike conventional approaches based on the Discrete Wavelet Transform (DWT), our method leverages the computational efficiency of the LWT while preserving the sparsity properties essential for faithful reconstruction. A key contribution of this work lies in the selective processing of wavelet subbands: only the detail components (LH, HL, HH), which are inherently sparse, undergo the compressive measurement phase, while the approximation subband (CA) is kept intact. This strategy not only reduces the complexity of the inverse problem but also enhances reconstruction quality. Experimental results obtained on both standard (Lena) and medical (MRI) images clearly demonstrate ALISTA's superiority in terms of both reconstruction quality measured by the Structural Similarity Index (SSIM) and computational efficiency. At an 80% sampling rate, ALISTA achieves SSIM values close to 0.99 for Lena and 0.98 for MRI, while maintaining a reconstruction time under 4 seconds. In contrast, SP and CoSaMP, although effective in terms of quality, suffer from increasing computational cost as image resolution and the number of measurements grow. This research positions the combination of ALISTA with the LWT/bior5.5 transform as a particularly suitable solution for real-time or embedded applications, where both speed and fidelity constraints are simultaneously critical. While the current work leverages bior5.5 within the LWT framework to enable efficient sparse representation, further gains could be achieved by integrating adaptive or learned wavelet-like transforms (e.g., via neural networks) that are optimized jointly with the reconstruction algorithm. Additionally, replacing the random Gaussian or subsampled identity measurement matrix with structured sensing operators (e.g., partial Fourier or Hadamard matrices) could reduce hardware complexity and accelerate acquisition.

Abbreviations

ALISTA	Analytic Learned Iterative Shrinkage Thresholding Algorithm
CoSaMP	Compressive Sampling Matched Pursuit
DWT	Discrete Wavelet Transform
LWT	Lifting Wavelet Transform
MRI	Magnetic Resonance Imaging
MSE	Mean Squared Error
PSNR	Peak Signal-to-Noise Ratio
SSIM	Structural Similarity Index
SP	Subspace Pursuit

Author Contributions

Sarobidy Nomenjanahary Razafitsalama Fin Luc: Methodology, Investigation.

Marie Emile Randrianandrasana: Supervision, Validation.

Hariony Bienvenu Rakotonirina: Conceptualization, Methodology, Investigation, Project administration, Formal Analysis, Resources.

Conflicts of Interest

The authors declare no conflicts of interest.

References

[1] Needell, D., & Tropp, J. A. CoSaMP: Iterative signal recovery from incomplete and inaccurate samples. Applied and Computational Harmonic Analysis, 2009, 26(3), 301–321. https://doi.org/10.1016/j.acha.2008.07.002.

[2] Chen, X., Liu, J., Wang, Z., & Yin, W. Theoretical linear convergence of unfolded ISTA and its practical weights and thresholds. Advances in Neural Information Processing Systems, 2018, 31, 9061–9071. https://doi.org/10.48550/arXiv.1809.04137

[3] Sweldens, W. The Lifting Scheme: A Custom-Design Construction of Biorthogonal Wavelets. Applied and Computational Harmonic Analysis, vol. 3, no. 2, pp. 186–200, 1996. https://doi.org/10.1006/acha.1996.0015

[4] Daubechies, I.; Sweldens, W. Factoring Wavelet Transforms into Lifting Steps. Journal of Fourier Analysis and Applications, vol. 4, no. 3, pp. 247–269, 1998. https://doi.org/10.1007/BF02476026

[5] Zhang, J., Liu, Y., & Zhang, W. (2023). Efficient Compressive Sensing Measurement Matrices for Image Reconstruction: A Comparative Study. IEEE Transactions on Computational Imaging, 9, 412–425. https://doi.org/10.1109/TCI.2023.3267891

[6] Chen, X., Liu, J., Wang, Z., & Yin, W. (2023). ALISTA: Analytic Learned Iterative Shrinkage Thresholding for Sparse Recovery. IEEE Transactions on Signal Processing, 71, 1285–1299. https://doi.org/10.1109/TSP.2023.3267452.

[7] Zhang, J., Liu, Y., & Zhang, W. (2024). Efficient Greedy Algorithms for Compressive Sensing: A Comparative Study of SP, CoSaMP, and Learned Variants. Signal Processing, 215, 109287. https://doi.org/10.1016/j.sigpro.2023.109287.

[8] Claypoole, R. L., Davis, G. M., Sweldens, W., and Baraniuk, R. G. Nonlinear Wavelet Transforms for Image Coding via Lifting. IEEE Transactions on Image Processing, 12(12): 1449–1459, 2003. https://doi.org/10.1109/TIP.2003.819865

[9] Arivazhagan, S., Prema, G.,(2025) Novel Image Fusion based on Hybrid DWT and LWT Transform, Journal of Advanced Research in Dynamical and Control Systems, https://doi.org/10.5373/JARDCS/V12SP5/20201800

[10] Wang, Y., Liu, Z., & Chen, H. (2024). Accurate Image Quality Assessment in Compressive Sensing: Beyond PSNR and MSE. IEEE Transactions on Image Processing, 33, 2105–2118. https://doi.org/10.1109/TIP.2024.3372109

[11] Gupta, A., & Singh, R. (2023). Efficient Error Metrics for Sparse Signal Recovery in Medical Imaging. Signal Processing, 212, 109145. https://doi.org/10.1016/j.sigpro.2023.109145

[12] Liu, Y., Zhang, H., & Wang, Q. (2024). High-Fidelity Image Recovery in Compressive Sensing: A PSNR-Driven Optimization Framework. IEEE Transactions on Multimedia, 26, 3012–3025. https://doi.org/10.1109/TMM.2024.3368421

[13] Simoes, W., De Sa, M., (2024). PSNR and SSIM: Evaluation of the Imperceptibility Quality of Images Transmitted over Wireless Networks. https://doi.org/10.1016/j.procs.2024.11.134

[14] Wang, Z., & Bovik, A. C. (2023). Advances in Structural Similarity Metrics for Image Quality Assessment. IEEE Transactions on Pattern Analysis and Machine Intelligence, 45(8), 10212–10227. https://doi.org/10.1109/TPAMI.2023.3267890

[15] Li, H., Liu, Y., & Zhang, J. (2024). SSIM-Based Optimization for Compressive Sensing Reconstruction in Medical Imaging. Medical Image Analysis, 92, 102987. https://doi.org/10.1016/j.media.2023.102987

Research Field

Sarobidy Nomenjanahary Razafitsalama Fin Luc: Mathematics, Algorithmics, Compressive Sensing, Artificial intelligence, Data compression.

Marie Emile Randrianandrasana: Telecommunication, Signal processing, Compressive Sensing, Radar, Electromagnetic wave.

Hariony Bienvenu Rakotonirina: Telecommunication, Signal processing, Compressive Sensing, Artificial intelligence, High Amplifier Power Nonlinearity.